ANL/UPD/CP-101520

The Structure of Tellurite Glass: A Combined NMR, Neutron Diffraction, and X-ray Diffraction Study

J. C. McLaughlin, S. L. Tagg, J. W. Zwanzier

Department of Chemistry, Indiana University, Bloomington, Indiana 47405

S. D. Shastri and D. R. Haeffner

User Program Division, Advanced Photon Source, Argonne National Laboratory, Argonne, IL 60439*

March 2000

To be presented at the 9th International Meeting on the Physics of Noncrystalline Solids, Tucson, Arizona, October 17-21, 2000; will be published in J. Non-Cryst. Solids.

*This work is supported by the U.S. Department of Energy, Basic Energy Sciences, Office of Science, under contract #W-31-109-ENG-38.

DISCLAIMER

DISCLAIMER

Portions of this document may be illegible in electronic image products. Images are produced from the best available original document.

The Structure of Tellurite Glass: A Combined NMR, Neutron Diffraction, and X-Ray Diffraction Study

J. C. McLaughlin* S. L. Tagg†

J. W. Zwanziger‡

Department of Chemistry, Indiana University, Bloomington, IN 47405

D. R. Haeffner

S. D. Shastri

Advanced Photon Source, Argonne National Laboratory, Argonne, IL 60439

Abstract

Models are presented of sodium tellurite glasses in the composition range $(Na_2O)_x$-$(TeO_2)_{1-x}$, $0.1 < x < 0.3$. The models combine self-consistently data from three different and complementary sources: sodium-23 nuclear magnetic resonance (NMR), neutron diffraction, and x-ray diffraction. The models were generated using the Reverse Monte Carlo algorithm, modified to include NMR data in addition to diffraction data. The presence in the models of all five tellurite polyhedra consistent with the Te^{+4} oxidation state were found to be necessary to achieve agreement with the data. The distribution of polyhedra among these types varied from a predominance of highly bridged species at low sodium content, to polyhedra with one or zero bridging oxygen

*Current Address: NIST, Gaithersburg, MD

†Current Address: Micron Technologies, Boise, ID

‡Corresponding author. Tel.: +1 812 855 3994; fax: +1 812 855 8500; e-mail: jzwanzig@indiana.edu

at high sodium content. The models indicate that the sodium cations themselves form sodium oxide clusters particularly at the $x = 0.2$ composition.

1 Introduction

Inorganic glasses possess complex structures which are intermediate between ordered materials and truly random systems [1]. A further complication is that almost all inorganic glasses of relevance include three or more chemical components. Therefore, a thorough investigation of the atomic-level structure must include methods that are sensitive to a range of length scales, due to the disorder, and to a range of atomic constituents. Because of these requirements, any one probe typically yields only limited information about the glass structure.

The purposes of this contribution are to describe a means for combining complementary data from diffraction experiments and nuclear magnetic resonance (NMR), and to present models of tellurite glasses. The systems of interest are the sodium tellurites, of general formula $(Na_2O)_x(TeO_2)_{1-x}$. Here TeO_2 is the glass-former and Na_2O is the modifier. The latter can be used to change various properties of the material, such as the glass transition temperature [2, 3] and the nonlinear optical response [4]. The ease of glass formation and subsequent stability against recrystallization in tellurites increases with alkali modifier content, up to about $x = 0.2$ and then decreases for $x > 0.2$. This effect is largest with sodium as the modifying cation [2].

The structural changes in tellurite glass due to modification have been the subject of numerous studies [2, 5–9]. There are two related issues: the binding sites and distribution of the modifier itself, and the resulting structure of the tellurium-oxygen network. Most work in this field has considered the latter problem. In the sodium tellurite system there are three crystalline compositions: $x = 20, 33$, and 50 mol-% Na_2O [10–12]. Together with TeO_2, these compositions bracket the glass forming range, which falls between about 5

and 35 mol-% Na_2O [2]. Five different tellurite polyhedra are found in these crystals [13] (Fig. 1). The crystal structures reveal that the coordination number of oxygen around tellurium is either 3 or 4 but that there is no change in the tellurium oxidation state. The conventional nomenclature for such polyhedra is Q^n, where the index n gives the number of bridging oxygen bonded to the central atom. In silicates and phosphates this nomenclature is sufficient, because not only the oxidation state but the coordination number in these glasses is fixed as well. For tellurite glasses, we extend this notation to Q^n_m, where the subscript m gives the coordination number. The resulting Q^n_m for each tellurite polyhedra can also be found in Fig. 1.

The distribution of tellurite polyhedra (Q^n_m, in our nomenclature) has been the subject of most structural work in this field. The neutron diffraction work of Neov [5] and Suzuki [6] established the importance of the $Q^4_4 \rightarrow Q^3_4$ transformation as a function of added modifier cation, where the Q^3_4 unit is usually understood to have a fourth oxygen nearby but not within true bonding range (often termed a TeO_{3+1} unit). Raman spectroscopy by Sekiya et al. [7], Tatsumisago et al. [14] and Himei et al. [15] provided more detailed models of the structural changes, including the possible presence of all the Q^n_m units found (subsequently) in the crystalline forms, with the exception of the Q^0_3 unit. Recently, Sakida et al. [9, 16] have published results of Te-125 NMR, which they interpret as indicating the presence of Q^4_4, Q^3_4, and Q^1_3 units. Q^2_3 units are rejected in their model based mainly on the fact that the theoretically predicted bands [17] for this unit are not found in the Raman spectra of the glasses.

The work reviewed above thus predicts that most of the Q species indicated in Fig. 1 are present in the glass, but does not make predictions as to the fraction present of each unit as a function of modifier. Moreover, the experiments cited give no direct information about the modifier environments and their distribution. In the following, by combining complementary techniques, we will provide models that answer both these questions.

2 Experimental Methods

2.1 Sample Preparation

Samples of sodium tellurite glasses were prepared by melting sodium carbonate and tellurite together at 800°C for 15 minutes. Glasses of composition $(Na_2O)_x(TeO_2)_{1-x}$ with $x = 0.12$, 0.15, 0.20, 0.25, and 0.28 were prepared for this study. The liquids were quenched between steel or brass plates. Sample composition was determined by weight-loss measurements and in some cases by electron microprobe analysis. The final compositions are precise to within $\pm 1\%$. The glass transition temperatures were found by differential scanning calorimetry and agreed within experimental error with previously published data [2].

2.2 Measurement Techniques

A variety of NMR experiments were used to measure the sodium chemical shift and the second moment, M_2, of the distribution of sodium-sodium dipolar couplings. These experiments are described in detail in several previous publications [18, 19]; here we use the measurements reported in those studies together with other experiments to develop new models of the glass structure. The sodium chemical shift gives information about the local environment of the sodium cations, because the shift can be related, empirically, to the number of near-neighbor oxygen [18, 20]. M_2 yields information about the spatial distribution of sodium, because it is related to the sodium-sodium pair distribution function through $M_2 = C \int g_{Na-Na}(r) r^{-6} 4\pi r^2 dr$, where all distance-independent quantities have been combined into the constant C. We call M_2/C the reduced second moment, and it is used as one of the fit parameters in the models. The data for sodium, determined by these methods, are listed in Table 1.

Neutron diffraction was measured on the Glass, Liquid, and Amorphous Diffractometer (GLAD) at the Intense Pulsed Neutron Source, Argonne National Laboratory (Fig. 2). This time-of-flight instrument has been described previously [21]. For each sample the total static

structure factor was extracted from the data using standard codes optimized for the GLAD instrument. The only non-standard feature used was a 0.286 Å cut-off of the neutron energy, to remove the tellurium neutron absorption resonance at 1.0 eV. For each sample the the total structure factor, $S(Q)$, was extracted after correcting the raw data for background artifacts, inelastic scattering, and multiple scattering, using the suite of programs designed for the GLAD instrument [21].

X-ray diffraction was performed on the Sector 1 bend-magnet beamline (1-BM), operated by the Synchrotron Research and Instrumentation Collaborative Access Team (SRI-CAT) at the Advanced Photon Source, Argonne National Laboratory (Fig. 2). 61.332 keV photons were used in order to be well above all absorption resonances, achieve wide Q-space coverage, and yield predominantly interior rather than surface diffraction. The photons were selected with a single Si (111) crystal with a 1.6° miscut. The crystal was bent (meridionally) to a monochromatic focus at the detector position. The monochromator crystal deflection was horizontal, while the scattering plane for the sample/detector was vertical in order to preserve acceptable angular resolution. A Ge solid-state detector was used. The structure factor, $F(Q)$, was extracted from the data, by correcting for Compton scattering, absorption, polarization, and background diffraction, following the procedure outlined by Williams [22]. The instrument dead-time was also measured and compensated for in the data analysis.

3 Results

As noted, the results from previously published NMR experiments used to make the models discussed below are summarized in Table 1. Example structure factors from neutron and x-ray diffraction, and the total pair distribution function derived from neutron diffraction, are shown in Fig. 2.

4 Discussion

Data from NMR, neutron diffraction, and x-ray diffraction were combined to generate real space models of the samples. Table 2 shows the weight factors of the different partial structure factors in the two diffraction experiments, and indicates why a variety of experiments is necessary to obtain a complete picture of the structure. Neutron diffraction probes mainly Te-O and O-O correlations, while x-rays are most sensitive to Te-Te and Te-O. NMR is necessary to probe the Na environments, including Na-O and Na-Na correlations. Together these three techniques provide enough information to generate realistic models of the glass.

Using the nomenclature established above, we describe the structures found in the tellurite crystals as follows. Crystalline TeO_2 has two isomorphs, paratellurite [23] (α-form) and tellurite [24] (β-form). Both forms are composed entirely of a fully interconnected network of 4 coordinate tellurium with 4 bridging oxygens each, or in the above notation, Q_4^4 polyhedra. The fully modified 50 mol-% Na_2O crystal [12] is composed of Q_3^0 polyhedra, which consist of a tellurium atom connected to 3 non-bridging oxygen resulting in a completely cleaved network. At the intermediate compositions of 20 and 33 mol-% Na_2O the network is only partially cleaved, and consists of a mixture of both 4 and 3 coordinate tellurite polyhedra. The 20 mol-% Na_2O crystal [10] still retains the Q_4^4 polyhedra found in pure TeO_2 but in addition has a number of bonds cleaved to form both Q_4^3 and Q_3^2 polyhedra. The 33 mol-% Na_2O crystal [11] contains none of the original Q_4^4 polyhedra and the network is composed of Q_4^3 polyhedra terminated by Q_3^1 polyhedra.

The crystal structures provide estimates for the bond lengths and minimum contact lengths (Table 2), and in fact these distances appear in the total pair distribution functions derived from the diffraction data (Fig. 2b). Coordination numbers of the atoms involved can be derived from these curves, but because of the complexity of the materials, both chemically and in terms of the range of possible structures (Fig. 1) uncertainties remain. What is evident from this analysis, however, is that the structures present in crystals are also present in the glass of similar composition.

To model the glass data, we used the Reverse Monte Carlo algorithm (RMC), described elsewhere [25, 26]. In our application, configurations with 3750 atoms at the proper density [2] (simulation cell roughly 40 Å/side) were generated and varied randomly, until agreement with a variety of imposed constraints was maximized. These constraints included both direct experimental data and indirect information on the chemical structures possible in such systems.

The direct experimental data included the total structure factor and total pair distribution function from neutron diffraction; the total structure factor from x-ray diffraction; the coordination number of oxygen about sodium, obtained from NMR [18]; and the M_2 constraint on the sodium distribution, also obtained from NMR [19]. Use of this last constraint is a new feature of RMC which we have added, and was accomplished by computing M_2/C after each move. This calculation is straightforward given the fact that $g_{Na-Na}(r)$ is calculated after each move as well.

The indirect information included closest approach distances of the various atomic pairs (Table 2) and coordination numbers of the tellurite groups (Fig. 1). Both types of information were obtained from study of the alkali tellurite crystal structures [10, 11, 13]. The distances used in the RMC models are about 10% less than the minimum comparable distances found in crystals, to allow disorder in the bond lengths. The coordination number constraints included those on sodium derived from NMR data and discussed above, and also constraints on tellurium and oxygen derived from crystal structures. Thus each oxygen was allowed to have 1 or 2 tellurium neighbors, and each tellurium either 3 or 4 oxygen neighbors (Fig. 1). No fractions were specified for these different possibilities. Additionally, the type of oxygen bonded to tellurium was constrained to correspond to the possibilities consistent with the oxidation state of the tellurium. Thus only Q_4^4 and Q_4^3 were allowed of the possible 4-coordinate tellurium, because species like Q_4^2 would require a change in oxidation state of tellurium, which is not observed. Likewise, all Q_3^n groups except Q_3^3 were allowed. Again, no compositional fractions were imposed on the distribution of Q groups. These types of

coordination constraints are also new features of RMC modeling which we have added.

The models were evolved using the RMC algorithm to convergence, which means in this context that the total mean square deviation of the model constraints from the target constraints is unchanging. The RMC fits, essentially superimposable with the data, are shown in Fig. 2. Providing a precise measure of the statistical significance of RMC fits is an open problem, because of the difficulty in counting the number of degrees of freedom in the constrained model. We take the models in Fig. 2 to be satisfactory representations of the data because they do not differ at any point from the data by more than the uncertainty in the data itself (error bars are shown at the right edge of all curves in Fig. 2).

We now discuss the structural features of the models. Fig. 3 shows a graph of the different Q_m^n species present in the simulations as a function of mol-% Na_2O. As the mol-% Na_2O increases, groups of lower coordination number appear at the expense of those with higher, indicating that the network is progressively cleaved. The original crystalline TeO_2 network is composed of TeO_4 trigonal bipyramids (Q_4^4). The fraction of tellurium atoms in Q_4^4 groups steadily decreases from about 40 to 20 % as the mol-% Na_2O increases. The Q_4^3 and Q_3^2 polyhedra, which maintain network connectivity while still possessing one non-bridging oxygen, together decrease steadily from about 35 to 25 %. The Q_3^1 and Q_3^0 groups reflect the breaking of the TeO_2 network, as they result in a terminating group or a lone TeO_3^{2-} group respectively. Based on the data for the Q_m^3 groups we suggest an underlying chemical equilibrium attained in the melt prior to quenching. As the modifier content is increased, the proportion of Q_2^3 first increases slightly, then decreases; next the Q_1^3 concentration increases, then decreases; and finally the Q_0^3 amount increases monotonically. These changes are indicative of an equilibrium distribution of all species in the liquid, with the identity of the average species shifting towards Q_0^3 at larger modifier content.

In contrast to the work cited in the introduction, we find that all five tellurite polyhedra are necessary to obtain models consistent with the full data sets presented here. For example, if the Q_3^2 unit is explicitly rejected, while all other units are permitted (again with no

constraints on their proportions) even limited ranges of the neutron and x-ray diffraction data cannot be fit. However, if only the x-ray or neutron data sets are used, a reduced set of polyhedra is sufficient to obtain a fit. We suggest that this finding indicates that any single data set, even of diffraction, can be expected to yield an incomplete picture of the structure of a multi-component glass.

The inter-connection of the Q_m^n groups is due to intermediate range order. We consider here the possible existence of rings, because rings are a common feature in crystalline tellurites [13]. For example, crystalline $Na_2Te_4O_9$ consists essentially of dimers joined through a four-membered Te-O ring (that is, a ring of two Te and two O atoms, alternating). Fig. 4 shows the distribution of rings found in the models of the glasses. The graph shows that rings, especially small rings, are not major components of the glass structure. Therefore, while the glass structure is consistent with the type of short-range order found in crystalline tellurites, the intermediate range order appears to be rather different. This difference may in fact be the reason for the stability of the glass with respect to de-vitrification even at the stoichiometric 20 mol-% modifier composition: a very substantial rearrangement is required to generate the small rings that are part of the crystal phases.

In addition to information on the network, our models give a detailed view of the incorporation of the modifier ion. We have previously [19] discussed models for the sodium ion distribution, and concluded that while a random hard sphere distribution captures the general increase in M_2 as a function of mol-% Na_2O it could not capture the larger increase in M_2 near the 20 mol-% composition. Introduction of the M_2 constraint into the RMC models now makes it possible to examine the sodium-sodium distribution in the context of a model which is also consistent with the diffraction data and other constraints imposed. The resulting $g_{Na-Na}(r)$ for the models is shown in Fig. 5. The resulting differences in the $g_{Na-Na}(r)$ parallels the larger change observed in M_2 (See Table 1 or Ref. 13) at the 20 mol-% Na_2O composition. The substantial change in modifier distribution at 20 mol-% Na_2O does not appear to affect the TeO_2 network modification or the bulk physical properties of

the glass, both of which change only gradually as a function of added modifier.

The glasses fall into two groups, with the break point at 20 mol-% Na_2O. The models at the smaller modifier concentration have a tendency towards cation separation. The minimum sodium-sodium contact distance in the models was 3.08 Å, but little intensity in $g(r)$ was measured until ~4.0 Å. These distributions are qualitatively different from hard-sphere distributions, which always have their maxima at the minimum approach distance. In contrast the models at higher modifier contents increase sharply near the minimum contact distance. Evidently, at lower modifier concentrations the sodium atoms are spatially anti-correlated, as compared to a hard-sphere distribution, while at higher concentrations the sodium atoms are found closer together. Thus this glass shows a significant structural change as a function of modifier, but one that is not strongly manifested in bulk properties such as density or T_g, because it is not closely related to the glass network. To our knowledge, this is the first report of such a sharp change in glass structure that is not reflected in the bulk thermal properties.

5 Conclusions

The five tellurite polyhedra found in crystalline alkali tellurites are all necessary to obtain models of the glasses consistent with a range of experimental data, including neutron diffraction, wide-angle x-ray diffraction, and sodium-23 NMR. Exclusion of any of the polyhedra results in models that do not simultaneously fit all the available data. The resulting models indicate a continuous cleavage of the tellurite network, with a composition of polyhedral types appropriate for chemical equilibria, probably frozen in from the liquid.

The intermediate range structure extracted from the models shows little in the way of rings; at the 20% modifier composition, the crystal form contains dimers linked by four-membered rings [10] while in the glasses only a few percent of the tellurium are involved in such rings. This difference implies that a very large structural rearrangement is necessary to

form the crystal from the glass, and which may explain the stability against de-vitrification at this composition [2].

The distribution of cations has a transition from avoidance, at concentrations less than 20 mol-%, to clustering at 20 mol-%, followed by a moderate decrease in clustering. As in superionic conductors, the ions appear to be de-coupled from the network, in that the glass transition is not affected by this change in the cation distribution, but unlike superionic conductors, here the cations are not significantly mobile [19]. Because the ion distribution has not been investigated in many glasses, this phenomenon of a substantial change in modifier ordering being decoupled from thermal properties may not be unique to this system.

Acknowledgements

We gratefully acknowledge assistance at IPNS of David Price, Ken Volin, Yaspal Badyal, and Jackie Johnson. This work was supported by the NSF under grant DMR-9508625 and DMR-9870246; work at the APS was supported by the U. S. Dept. of Energy, BES-Materials Sciences, under contract No. W-31-109-ENG-38.

References

[1] S. R. Elliott, Physics of Amorphous Materials. Wiley, New York, 2nd edition (1990).

[2] J. Heo, D. Lam, G. H. Sigel, Jr., E. A. Mendoza, D. A. Hensley, J. Am. Ceram. Soc. 75 (1992) 277.

[3] M. Zhang, S. Mancini, W. Bresser, P. Boolchand, J. Non-Cryst. Solids 151 (1992) 149.

[4] R. El-Mallawany, J. Appl. Phys. 72 (1992) 1774.

[5] S. Neov, V. Kozhukharov, I. Gerasimova, K. Krezhov, B. Sidzhimov, J. Phys. C 12 (1979) 2475.

[6] K. Suzuki, J. Non-Cryst. Solids 95-96 (1987) 15.

[7] T. Sekiya, N. Mochida, A. Ohtsuka, M. Tonokawa, J. Non-Cryst. Solids 144 (1992) 128.

[8] M. Tatsumisago, S.-K. Lee, T. Minami, Y. Kowada, J. Non-Cryst. Solids 177 (1994) 154.

[9] S. Sakida, S. Hayakawa, T. Yoko, J. Non-Cryst. Solids 243 (1999) 13.

[10] S. L. Tagg, J. C. Huffman, J. W. Zwanziger, Chem. Mater. 6 (1994) 1884.

[11] S. L. Tagg, J. C. Huffman, J. W. Zwanziger, Acta Chem. Scand. 51 (1997) 118.

[12] R. Masse, J. C. Guitel, I. Tordjman, Mat. Res. Bull. 15 (1980) 431.

[13] C. R. Becker, S. L. Tagg, J. C. Huffman, J. W. Zwanziger, Inorg. Chem. 36 (1997) 5559.

[14] M. Tatsumisago, T. Minami, Y. Kowada, H. Adachi, Phys. Chem. Glasses 35 (1994) 89.

[15] Y. Himei, A. Osaka, T. Nanba, Y. Miura, J. Non-Cryst. Solids 177 (1994) 164.

[16] S. Sakida, S. Hayakawa, T. Yoko, J. Non-Cryst. Solids 243 (1999) 1.

[17] T. Uchino T. Yoko, J. Non-Cryst. Solids 204 (1996) 243.

[18] S. L. Tagg, R. E. Youngman, J. W. Zwanziger, J. Phys. Chem. 99 (1995) 5111.

[19] J. W. Zwanziger, J. C. McLaughlin, S. L. Tagg, Phys. Rev. B 5 (1997) 5243.

[20] H. Koller, G. Engelhardt, A. P. M. Kentgens, J. Sauer, J. Phys. Chem. 98 (1994) 1544.

[21] A. J. G. Ellison, R. K. Crawford, D. G. Montague, K. J. Volin, D. L. Price, J. Neutron Res. 1 (1993) 61.

[22] A. Williams, X-ray Diffraction Studies of Metallic Glasses, Ph.D. thesis, California Institute of Technology, Pasadena, California (1980).

[23] O. Lindqvist, Acta Chem. Scand. 22 (1968) 977.

[24] H. Beyer, Z. Kristallogr. 124 (1967) 228.

[25] R. L. McGreevy, L. Pusztai, Mol. Simulation 1 (1988) 359.

[26] J. D. Wicks, Studies of disordered materials, Ph.D. thesis, Oxford University, Oxford, U. K. (1993).

Tables

Table 1: Structural data derived from NMR measurements, used in construction of real-space models. The first column gives the sample composition; the second, the average coordination number of oxygen around sodium, as derived from the sodium chemical shift; and the third, the reduced sodium dipolar second moment, as measured in spin-echo decay experiments.

mol-% Na_2O	Avg. CN	M_2/C ($\times 10^{-3}$Å^{-6})
12	5.8	0.75
15	5.8	0.88
20	5.5	3.74
25	5.4	3.95
28	5.4	4.29

Table 2: For each atom pair, the closest approach distance R_{min} used in the RMC models is given. These values are about 10% less than the shortest comparable distances found in crystalline tellurites. Given also are the Faber-Ziman weighting coefficients of each atom pair in the total neutron structure factor, and the comparable weights at $q = 0$ in x-ray diffraction.

Atom Pair	R_{min} (Å)	Neutron weight	X-ray weight ($q = 0$)
Te-Te	3.08	0.079	0.481
Te-Na	3.16	0.049	0.098
Te-O	1.68	0.355	0.327
Na-Na	3.08	0.007	0.005
Na-O	2.16	0.110	0.033
O-O	2.48	0.400	0.056

Figure Captions

Figure 1: Tellurite structures found in the $x = 0.20$, $x = 0.33$, and $x = 0.50$ sodium tellurite crystals. We adopt a terminology where each structural unit is identified in term of Q^n_m, where $m = 3, 4$ and identifies the total number of oxygen bonded to the tellurium atom, and $n = 0$–4 is the number of bridging oxygen bonded to the tellurium atom.

Figure 2: A typical set of diffraction data used to construct the models. Shown are: (a) $S(Q)$ from neutron diffraction; (b) $G(r)$, obtained from $S(Q)$ by a Monte Carlo-based inversion; and (c) $F(Q)$ from wide-angle x-ray diffraction (because of the Q-dependence of the x-ray form factors, this data was not inverted). The error bars for the data are indicated at the far right of each plot. Each graph also includes the same quantities derived from the RMC models, which in each case is nearly super-imposable with the data. The data is for the $(Na_2O)_{0.2}(TeO_2)_{0.8}$ composition. Data derived from NMR were used simultaneously in the fits, and are listed in Table 1.

Figure 3: Proportion of the Q^n_m species found in the models. ■: Q^4_4; ●: Q^3_4; ○: Q^2_3; ▲: Q^1_3; △: Q^0_3. The lines connecting points are provided only as guides to the eye.

Figure 4: Rings per 100 Te atoms found in the models of the glasses, as a function of modifier content. Ring size: ■ 4; □ 6; ● 8; ○ 10 and ▲ 12. The lines connecting points are provided only as guides to the eye.

Figure 5: The sodium-sodium pair distribution function from the RMC models using the NMR data.

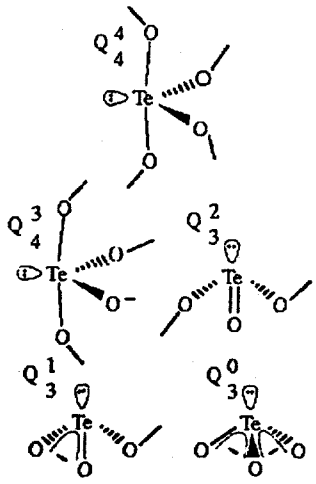

McLaughlin et al.
Fig. 1

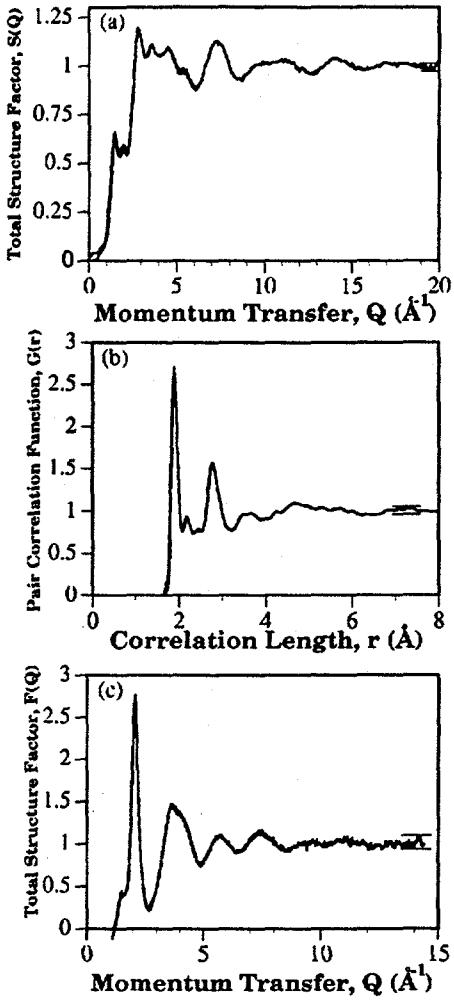

McLaughlin et al. Fig. 2

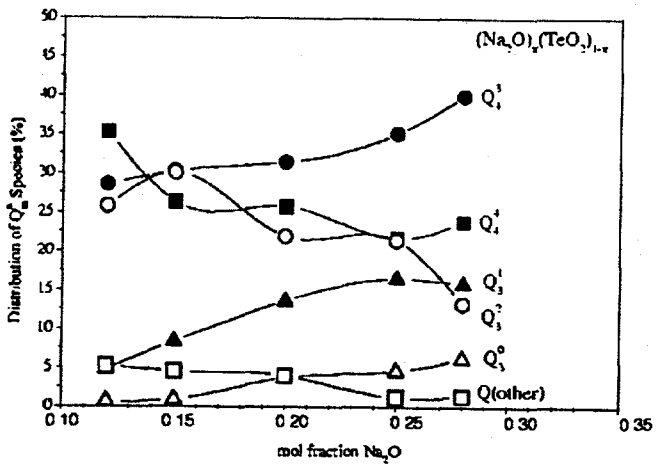

McLaughlin et al.
Fig. 3

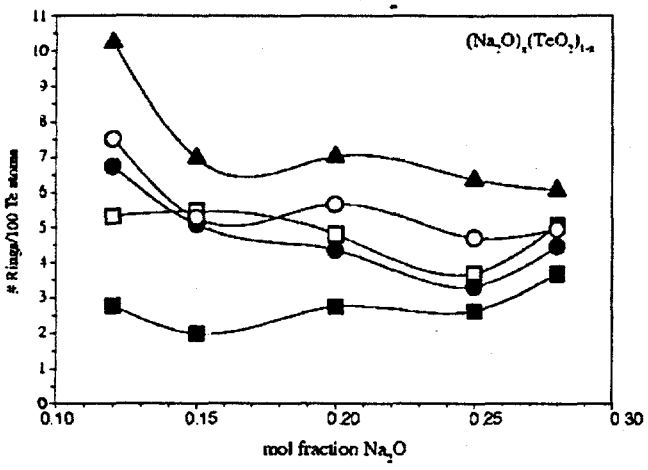

McLaughlin et al.
Fig. 4

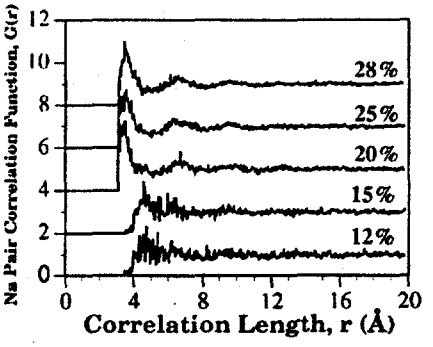

McLaughlin et al
Fig. 5